nature physics

LETTERS

PUBLISHED ONLINE: 1 APRIL 2012 | DOI: 10.1038/NPHYS2277

Phonon-cavity electromechanics

I. Mahboob*, K. Nishiguchi, H. Okamoto and H. Yamaguchi*

Photonic cavities have emerged as an indispensable tool to control and manipulate harmonic motion in opto/electromechanical systems[1]. Invariably, in these systems a high-quality-factor photonic mode is parametrically coupled to a high-quality-factor mechanical oscillation mode[2–12]. This entails the demanding challenges of either combining two physically distinct systems, or else optimizing the same nanostructure for both mechanical and optical properties[4–11]. In contrast to these approaches, here we show that the cavity can be realized by the second oscillation mode of the same mechanical oscillator[13,14]. A piezoelectric pump[15,16] generates strain-induced parametric coupling between the first and the second mode at a rate that can exceed their intrinsic relaxation rate. This leads to a mechanically induced transparency in the second mode which plays the role of the phonon cavity[17,18], the emergence of parametric normal-mode splitting[19,20] and the ability to cool the first mode[2–11]. Thus, the mechanical oscillator can now be completely manipulated by a phonon cavity[21].

The dynamical backaction of a photonic cavity that is parametrically coupled to a mechanical oscillation mode has recently led to the realization of a quantized macroscopic mechanical system[10,11,22–24], a long-standing goal in solid-state physics[25]. The backaction of the mechanical motion on the cavity has also resulted in the emergence of opto/electromechanically induced transparency, which has great potential for communications technology and quantum information science[17,18,20,26–28].

The success of this approach is leveraged on the requirement that the mechanical oscillation completes many cycles before the cavity relaxes, thus enhancing the effectiveness of the dynamical backaction, or in other words the coupled system is operated in the resolved sideband regime[1,22,23]. The parametric coupling in these systems arises from the harmonic motion of the mechanical element modifying the cavity's resonance frequency by means of a change in either the cavity's length or capacitance. This has resulted in exquisitely engineered devices in which the mechanical motion can be manipulated by the parametrically coupled photonic cavity[1].

In contrast to a photonic cavity, a phonon cavity operated in the resolved sideband regime should also be able to host dynamical backaction onto the mechanical element. One approach to this goal could be realized by physically coupling an additional mechanical oscillator to the system. Here we show that a more natural method is to simply couple two different colour mechanical oscillation modes in the same mechanical system, where the first mode represents the mechanical oscillation of interest and the second mode affords a phonon cavity. The key to this approach is a geometric intermodal coupling, where the motion of the first (second) mode creates tension that causes a shift in the frequency of the second (first) mode, that can be parametrically manipulated[29,30], which enables phonon-cavity electromechanics to be realized[1,20].

The electromechanical resonator used in this study is shown in Fig. 1a and described in detail elsewhere[15,16]. It hosts flexural oscillation modes that are transduced by the piezoelectric

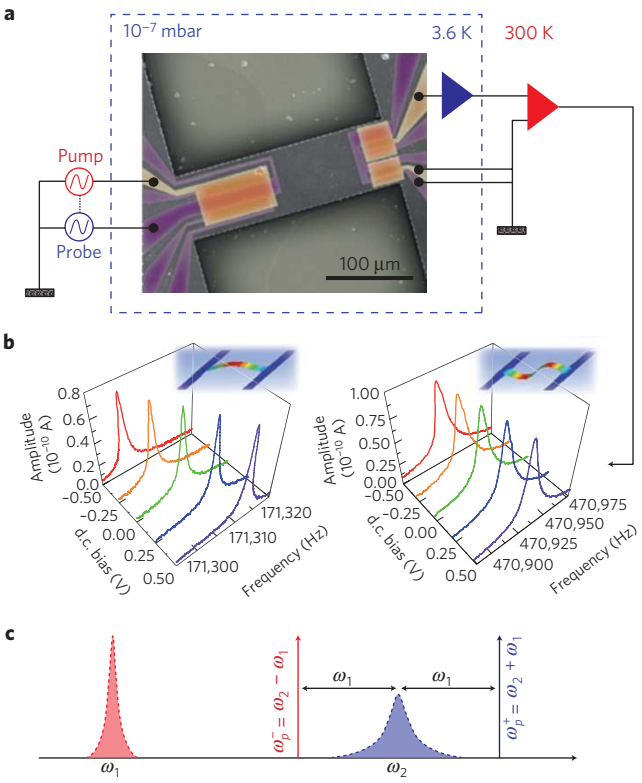

Figure 1 | The phonon-cavity electromechanical system. a, A false-colour electron micrograph of the mechanical resonator sustaining a two-dimensional electron gas (purple) above which Schottky-contacted gold electrodes (orange) are located. The piezoelectric effect between them transduces the mechanical motion. Also shown is a simplified measurement circuit, where the harmonic probe is used to investigate the first mode or the phonon cavity and the pump which dynamically couples them. The mechanical-motion-induced piezovoltage is first amplified on-chip then at room temperature and is measured using either a lock-in or a spectrum analyser. **b**, The phonon-cavity electromechanical system, harmonically probed with an amplitude of 100 $\mu V_{r.m.s.}$ and 3 $mV_{r.m.s.}$, reveals the first mode and the second mode (that is, the phonon cavity), respectively, as function of d.c. bias instead of the pump as depicted in **a** (simulated mode profiles are also shown in the insets). The d.c. bias generates piezoelectric strain which modifies their eigenfrequencies and it can be exploited to enhance the parametric intermodal coupling. **c**, A schematic profile of the phonon-cavity electromechanical system, where the mechanical motion of interest is given by the first mode ω_1, the second mode ω_2 plays the role of the phonon cavity and the anti-Stokes (Stokes) pump that dynamically couples them when activated at ω_p^- (ω_p^+).

effect, where the first mode $\omega_1/2\pi = 171.3$ kHz with damping $\gamma_1/2\pi = \omega_1/2\pi Q_1 = 1.1$ Hz (Q is the quality factor) and the second

NTT Basic Research Laboratories, NTT Corporation, Atsugi-shi, Kanagawa 243-0198, Japan. *e-mail: imran.mahboob@lab.ntt.co.jp; yamaguchi.hiroshi@lab.ntt.co.jp.

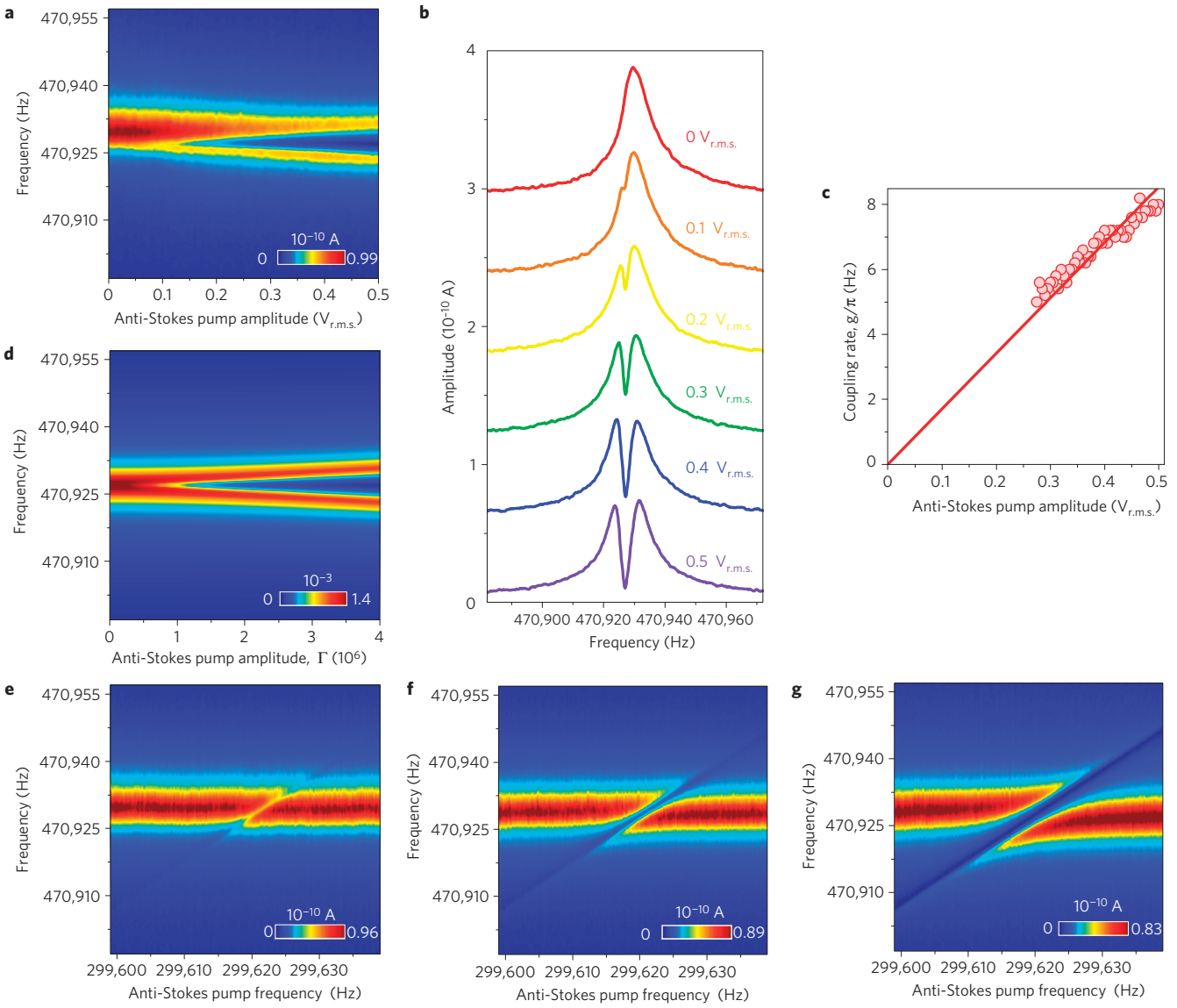

Figure 2 | The phonon-cavity dynamics. a,**b**, The phonon cavity's response as a function of the anti-Stokes pump amplitude at ω_p^- where all the spectra are offset for clarity in **b**. For weak pump amplitudes, phonons are converted from the phonon cavity to the first mode, resulting in a dip in its response (that is, the phonon cavity has a mechanically induced transparency). By increasing the pump amplitude further, the parametric coupling is enhanced and the phonon cavity begins to hybridize with the first mode, undergoing parametric normal-mode splitting (note the phonon cavity undergoes a thermal drift for large pump amplitudes owing to current leakage between the top-gate and the two-dimensional electron gas). **c**, The coupling rate extracted from **a** (points) reveals a linear dependence on the anti-Stokes pump amplitude and is confirmed by a least squares fit (line). **d**, The numerical solution to equation (1) for the conditions described in **a** confirms the experimental result, albeit without the thermal drift. **e**–**g**, The spectroscopy of the parametric coupling via the phonon cavity with the anti-Stokes pump amplitudes $V_p = 0.125$, 0.25 and 0.5 $V_{r.m.s.}$ respectively. As the coupling between the first mode and the phonon cavity is increased, it results in the characteristic anti-crossing of strongly coupled systems.

mode $\omega_2/2\pi = 470.93$ kHz with $\gamma_2/2\pi = \omega_2/2\pi Q_2 = 8.5$ Hz, which henceforth will be known as the phonon cavity (see Fig. 1b). This data indicates ultra-deep resolved sideband operation with an unprecedented ratio $\omega_1/\gamma_2 \approx 2 \times 10^4$, which is orders of magnitude larger than photon-based counterparts[1–11,14,22,23].

In the phonon-based system and in contrast to photon-cavity electromechanical systems, the motion of the first mode induces tension that can modify the frequency of the phonon cavity, creating sidebands at $\omega_2 \pm \omega_1$, as schematically depicted in Fig. 1c (ref. 1). The coupling strength $G = \mathrm{d}\omega_2/\mathrm{d}X_1$ quantifies the degree of parametric intermodal coupling and is given by the tension-induced change in the phonon-cavity frequency for a given displacement of the first mode (see Supplementary Information for an illustrative example)[20,30].

On the other hand, application of d.c. bias also enables the frequency of the first mode and the phonon cavity to be manipulated via piezoelectrically induced tension, which yields $\delta\omega_1/2\pi = 11\ \mathrm{Hz\,V^{-1}}$ and $\delta\omega_2/2\pi = 6\ \mathrm{Hz\,V^{-1}}$ respectively, as shown in Fig. 1b (ref. 15). Consequently, if the system is periodically pumped (ω_p) by a sufficiently large bias (V_p) it can not only modulate the eigenfrequency of both the first mode and the phonon cavity as $\delta\omega_n V_p \cos(\omega_p t)$, where $n = 1$ or 2 respectively, but it can also drive the parametric coupling between them. For example, the pump can induce a change in the displacement of the first mode, which in turn modifies the tension and thus the frequency and energy of the phonon cavity. The relaxation time ($1/\gamma_2$) delayed response of the phonon cavity results in a backaction force on the first mode via the same coupling mechanism modifying its oscillation dynamics[1,14].

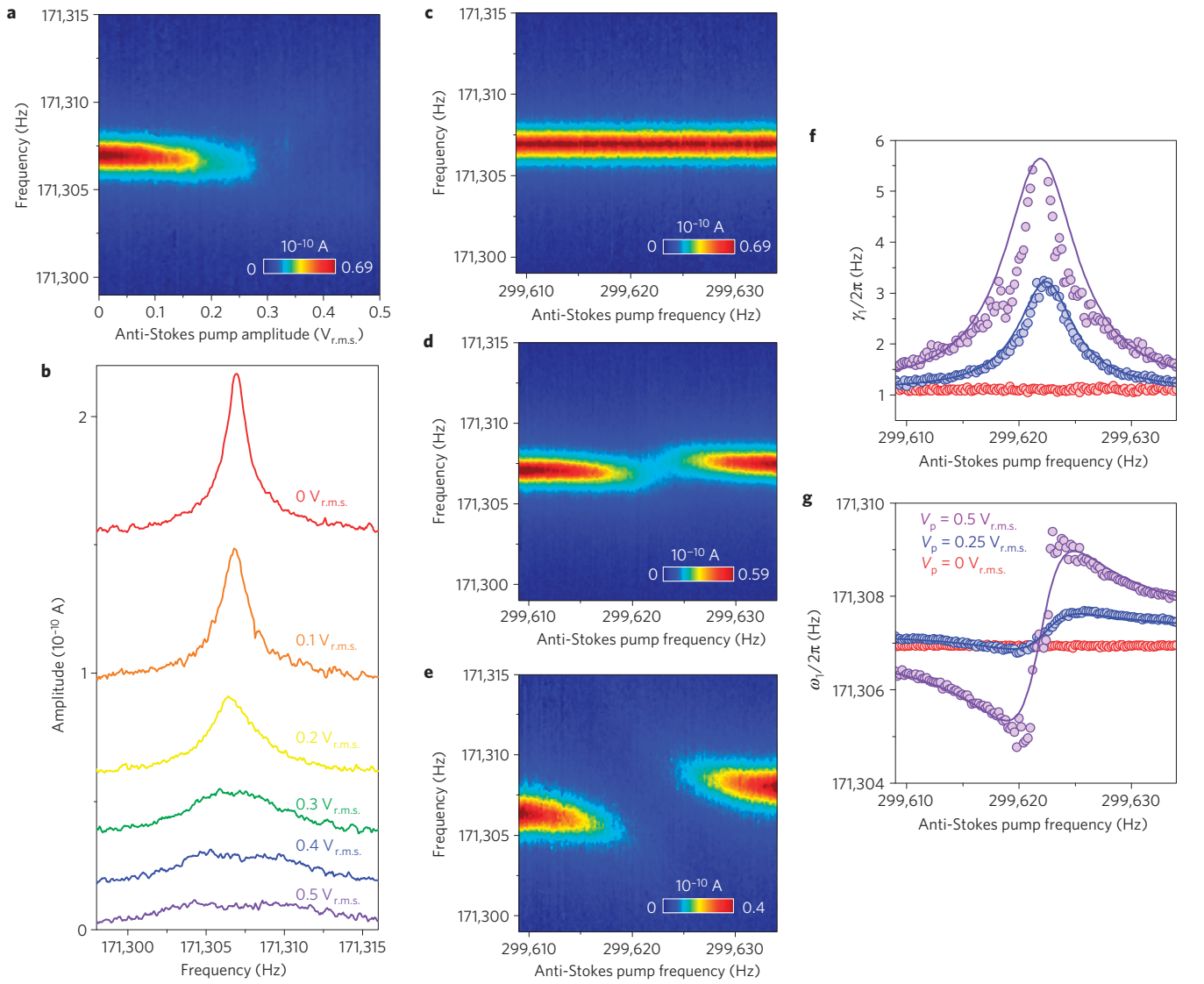

Figure 3 | The backaction of the phonon cavity on the first mode. a,**b**, The response of the first mode to the anti-Stokes pump at ω_p^-. As the pump amplitude is increased, phonons are transferred from the first mode to the phonon cavity, resulting in X_1 decreasing and γ_1 increasing. At the strongest pump amplitudes the parametric coupling is amplified, resulting in the emergence of normal-mode splitting in the response of the first mode. Note all the spectra are offset for clarity in **b**. **c**–**e**, The spectroscopy of the phonon-cavity electromechanical system via the first mode as a function of the anti-Stokes pump detuning and amplitude at 0, 0.25 and 0.5 $V_{r.m.s.}$ respectively reveals its transformation as it is more strongly coupled to the phonon cavity. **f**,**g**, γ_1 and ω_1 as a function of the anti-Stokes pump frequency (points) clearly reveal signatures of the in-phase and quadrature components of the phonon cavity in the response of the first mode. Also shown are theoretical fits for the dynamical backaction (lines), as described in the main text.

The parametric coupling and the dynamical backaction effects can be greatly enhanced when $\omega_p^- = \omega_2 - \omega_1$ ($\omega_p^+ = \omega_2 + \omega_1$) and pumping on the anti-Stokes/red sideband (Stokes/blue sideband) can damp (amplify) the first mode (Fig. 1c)[29].

In this configuration, the Hamiltonian of the coupled system can be expressed as

$$H = \sum_{n=1}^{2}\left(P_n^2/2m_n + m_n\omega_n^2 X_n^2/2\right) - \Lambda X_2\cos(\omega_s t) - \sum_{n=1}^{2}\left((\Delta_n X_n^2/2)\cos(\omega_p t)\right) - gX_1X_2\cos(\omega_p t) \quad (1)$$

where the first two terms are the kinetic and potential energies respectively, with canonical coordinates X_n and P_n denoting the position and conjugate momentum of the constituent systems with mass m_n. Λ is the amplitude of the harmonic probe of the phonon cavity with $\omega_s \approx \omega_2$. Δ_n is proportional to the piezoelectric pump amplitude, where this term arises from piezoelectric frequency pulling of the mechanical resonator, and it results in parametric resonance when $\omega_p = 2\omega_n$ (ref. 15). The combination of the terms with Λ and Δ_2 can also permit degenerate/non-degenerate parametric amplification and squeezing when $\omega_p \approx 2\omega_2$ (refs 16,31). The last term describes the linearized parametric coupling between the first mode and the phonon cavity[20,32], where the coupling rate $g \propto GV_p$, and this becomes the dominant term when $\omega_p = \omega_p^{\pm}$. Thus the term containing Δ_n can be neglected in the present investigation.

To probe the phonon cavity, a weak harmonic excitation (3 $mV_{r.m.s.}$) is applied at $\omega_s \approx \omega_2$ and the system is pumped on the red sideband at ω_p^- whilst the pump amplitude is increased. In this configuration, the phonons from the pump and in the phonon cavity are annihilated whilst phonons are created in the first mode to conserve energy[29]. The numerical solution to equation (1) (Fig. 2d and Methods) confirms that the phonon cavity transfers energy to the first mode, and when $g \approx \sqrt{\gamma_1\gamma_2}$ it results in a

mechanically (that is, phonon) induced transparency in the phonon cavity[17,18,20,27,28]. As the pump amplitude is increased further, the condition $g \geq \gamma_2 \gg \gamma_1$ can be satisfied, and the system enters the strong-coupling regime. In this limit, the phonon cavity and the first mode can no longer be considered as distinct entities, but rather as a composite of their initial eigenmodes, and will undergo parametric normal-mode splitting; a widely observed phenomenon in strongly coupled systems[19,20,25,32].

The experimental results shown in Fig. 2a,b confirm this assertion, where the phonon cavity becomes transparent at pump amplitudes of 0.3 $V_{r.m.s.}$. As the pump amplitude is increased further the system exhibits the emergence of parametric normal-mode splitting and the peak separation given by $2g$ enables the coupling rate to be extracted, as shown in Fig. 2c (ref. 20). This reveals g/π can be linearly increased by the anti-Stokes pump to 8 Hz, placing the system on the cusp of the strong coupling regime[19,20].

Alternatively, detuning the anti-Stokes pump frequency and probing the phonon cavity reveals the presence of the first mode, as shown in Fig. 2e–g. As the first mode's sideband approaches the phonon cavity it acquires its damping rate and becomes broader. This effect is enhanced as the anti-Stokes pump amplitude is increased and results in the avoided-crossing characteristic of strongly coupled systems, namely the first mode and the phonon cavity. Numerical simulations using equation (1) (see Methods) can easily reproduce the above spectroscopy and are shown in the Supplementary Information.

The phonon-cavity electromechanical system can also be excited by the Stokes pump, where this process creates phonons in both the phonon cavity and the first mode at the expense of the pump phonons, and is described in detail in the Supplementary Information[33].

The intermodal parametric coupling can be engineered to control and manipulate the first mode by means of the phonon cavity. By pumping on the red sideband at ω_p^-, the first mode is probed with a weak (100 $\mu V_{r.m.s.}$) harmonic excitation as a function of the pump amplitude, as shown in Fig. 3a,b. In this configuration, the phonons from the anti-Stokes pump and in the first mode are annihilated whilst phonons are created in the phonon cavity. Consequently, the energy and hence the area associated with the spectral response of the first mode decreases, as shown in Fig. 4d. Moreover, as the anti-Stokes pump amplitude is increased, the enhanced coupling between the first mode and the phonon cavity results in Q_1 being greatly reduced, as shown in Fig. 4c. For the strongest pump amplitudes, the coupling reaches a point where parametric normal-mode splitting can even be observed in the first mode and its behaviour can no longer be characterized by a single harmonic oscillator response function[19].

On the other hand, if the anti-Stokes pump is detuned, the phonon cavity's dynamics can be imprinted onto the first mode, where γ_1 and ω_1 trace out its in-phase and quadrature components, as shown in Fig. 3c–g. For a pump amplitude of 0.5 $V_{r.m.s.}$, $\gamma_1/2\pi$ tends to $(\gamma_1+\gamma_2)/4\pi$ ~5 Hz; concurrently $\omega_1/2\pi$ also undergoes a 5 Hz shift (Fig. 3f,g). From the theory of photon-based opto/electromechanical systems operated in the resolved sideband regime, the change in ω_1 and γ_1 can be expressed as $4g^2\delta/(\gamma_2^2+4\delta^2)$ and $4g^2\gamma_2/(\gamma_2^2+4\delta^2)$ respectively, where the pump detuning about ω_p^- is given by δ (refs 20,22,23). We find that this formalism is equally applicable to the phonon cavity realized here and it can reproduce the experimental response as shown in Fig. 3f,g approximately using the experimentally determined values for g and γ_2.

Invariably, the dynamical backaction of the photonic cavity has been employed to cool a mechanical oscillation mode[1–11,22–24]. Here we show that this concept can also be applied to the phonon cavity. A white noise voltage corresponding to a displacement $X_1' = 0.37$ nm (see Methods and Supplementary Information) and temperature $T' \gg 3.6$ K is injected into the spectral region around the first mode, as shown in Fig. 4a,b. Activating the anti-Stokes pump at ω_p^- transfers phonons corresponding to the displacement noise energy of the first mode to the phonon cavity, where a stronger pump amplitude enhances the transfer rate. For the largest pump amplitude, almost all the displacement noise energy is transferred to the phonon cavity, resulting in the temperature T and hence X_1 and Q_1 of the first mode reducing (Fig. 4c,d). The normalized temperature $T/T' = \int X_1^2(\omega)\mathrm{d}\omega / \int X_1'^2(\omega)\mathrm{d}\omega$ at various pump amplitudes indicates that the temperature of the first mode can be reduced by a factor of ~2 by means of the dynamical backaction of the phonon cavity, as shown in Fig. 4d. The measured response of T and Q_1 as a function of the anti-Stokes pump amplitude can be reproduced through equation (1) and is detailed in the Supplementary Information. The strong pump also results in thermal drift (Fig. 2a) but a corresponding increase in the noise temperature is not observed, as it is obscured by the very large T' and by the noise floor temperature from the room temperature amplifier.

At an ambient temperature of 3.6 K (that is, without the white noise) the parametric coupling will result in the phonon number,

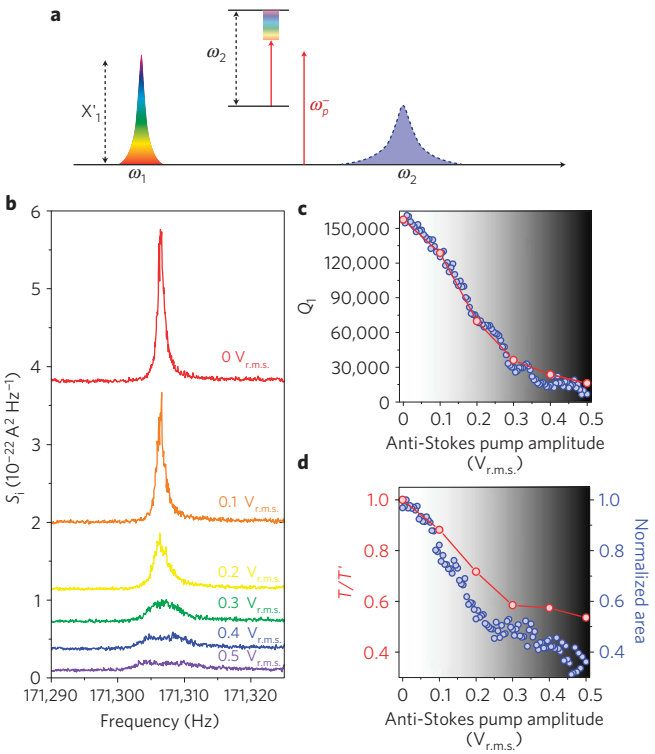

Figure 4 | Cooling the first mode via the phonon cavity. a, A white noise displacement X_1' corresponding to a temperature $T' \gg 3.6$ K is injected into a narrow bandwidth around the first mode. Concurrently, the anti-Stokes pump is activated at ω_p^-, which results in the displacement noise energy from the first mode being transferred to the phonon cavity, cooling the fundamental mechanical oscillation in the process. **b**, The power spectral density of the first mode as a function of the pump amplitude clearly reveals its area and, hence, temperature is reduced as it is more strongly coupled to the phonon cavity. At the largest pump amplitudes, the emergence of parametric normal-mode splitting can even be observed in the response of the first mode. Note all the spectra are offset for clarity. **c**,**d**, The corresponding Q_1 and T/T' respectively extracted from the above measurement as a function of the anti-Stokes pump amplitude (red points). Also shown are Q_1 and the normalized area extracted from Fig. 3a (blue points), confirming the trends observed in the noise measurement. For a pump amplitude of more than 0.3 $V_{r.m.s.}$ (shaded region) normal-mode splitting can be observed in the response of the first mode, resulting in it no longer being described by a single harmonic oscillator response function.

$N_n = k_b T/\hbar\omega_n$, where k_B is the Boltzmann constant, of the first mode and the phonon cavity converging to $(N_1+N_2)/2$. This will result in a first mode temperature of 2.4 K. To achieve cooling beyond this requires the phonon cavity to be realized at a much higher frequency, namely $N_2 \ll 1$. Consequently, even though the phonon cavity permits dynamical backaction on to the first mode it is ill-suited to cool it into its quantum ground state, that is, $N_1 < 1$. This objective is much more successfully served by photonic cavities which can be initialized in their quantum ground state by virtue of their higher operation frequencies[10,11].

However, the novelty of the present approach lies in the unprecedented ability to parametrically manipulate mechanical nonlinearities, as demonstrated previously with the present system[15,16,31], to engineer novel Hamiltonians (equation (1)). Ultimately, this will enable phonons to be squeezed[34] and entangled in two different colour states[13] when the mechanical oscillation modes are operated in their quantum ground state[10,11,25]. Indeed, this phenomenon is not limited only to piezoelectric transducers and it can be generalized to any scheme that can modulate the eigenfrequencies of the first mode and the phonon cavity, enabling the intrinsic intermodal coupling to be exploited. Consequently, this work opens up a new direction for opto/electromechanical systems that inherently incorporate phonon cavities, which promises hitherto unconsidered prospects[34].

Methods

Experimental. The electromechanical resonator was fabricated by conventional micromachining processes from a GaAs/AlGaAs modulation-doped heterostructure sustaining a two-dimensional electron gas 90 nm below the surface. The sample was mounted in a high-vacuum insert which was then placed in a ^{4}He cryostat.

The pump and probe excitations were generated from a single signal generator with two synchronized outputs (NF Wavefactory 1966). A homodyne measurement scheme was employed and the electromechanical oscillator's response was amplified by an on-chip Si-nano-field-effect-transistor with a 25 dB gain, followed by a transimpedance amplifier (Femto DLPCA-200) with a gain of 10^6 VA^{-1}, and measured in a lock-in amplifier (Ametek 7265). A spectrum analyser with a built-in random noise source was used for the noise measurements (Agilent 89410A).

Numerical simulations. The equations of motion of the parametrically coupled modes ω_2 and ω_1 can be extracted from equation (1) as $\partial H/\partial P_n = \dot{X}_n$ and $-\partial H/\partial X_n = \dot{P}_n$, using the identity $P_n = m_n\dot{X}_n$, giving

$$\ddot{X}_2 + \frac{\omega_2}{Q_2}\dot{X}_2 + \omega_2^2 X_2(1+\beta_2 X_2^2) = \Lambda\cos(\omega_s t) + \Gamma X_1\cos(\omega_p t) \quad (2)$$

$$\ddot{X}_1 + \frac{\omega_1}{Q_1}\dot{X}_1 + \omega_1^2 X_1(1+\beta_1 X_1^2) = \Gamma X_2\cos(\omega_p t) \quad (3)$$

where $\omega_s = \omega_2 + \delta_s$ and $\omega_p = \omega_p^- + \delta_p$. Dissipation terms parameterized by Q_n, the Duffing nonlinearity defined by β_n and a generic pump amplitude Γ in lieu of g have also been introduced and, for simplicity, the mass of both modes is set to unity. Equations (2) and (3) are solved in the rotating frames at ω_2 and ω_1 respectively by decomposing X_2 and X_1 to

$$X_2(t) = a_2(t)\sin(\omega_2 t) + b_2(t)\cos(\omega_2 t) \quad (4)$$

$$X_1(t) = a_1(t)\sin(\omega_1 t) + b_1(t)\cos(\omega_1 t) \quad (5)$$

where $a_2(t)$, $b_2(t)$, $a_1(t)$ and $b_1(t)$ are slowly varying compared with ω_2 and ω_1 respectively. Using equations (4) and (5), equations (2) and (3) can thus be expressed as

$$\dot{a}_2(t) = \frac{1}{2\omega_2}\left(-\frac{\omega_2^2 a_2(t)}{Q_2} - \frac{3}{4}\beta_2\omega_2^2 b_2(t)(a_2^2(t)+b_2^2(t)) + \Lambda\cos(\delta_s t) + \frac{\Gamma b_1(t)}{2}\cos(\delta_p t) - \frac{\Gamma a_1(t)}{2}\sin(\delta_p t)\right) \quad (6)$$

$$\dot{b}_2(t) = \frac{1}{2\omega_2}\left(-\frac{\omega_2^2 b_2(t)}{Q_2} + \frac{3}{4}\beta_2\omega_2^2 a_2(t)(a_2^2(t)+b_2^2(t)) + \Lambda\sin(\delta_s t) - \frac{\Gamma b_1(t)}{2}\sin(\delta_p t) - \frac{\Gamma a_1(t)}{2}\cos(\delta_p t)\right) \quad (7)$$

$$\dot{a}_1(t) = \frac{1}{2\omega_1}\left(-\frac{\omega_1^2 a_1(t)}{Q_1} - \frac{3}{4}\beta_1\omega_1^2 b_1(t)(a_1^2(t)+b_1^2(t)) + \frac{\Gamma b_2(t)}{2}\cos(\delta_p t) + \frac{\Gamma a_2(t)}{2}\sin(\delta_p t)\right) \quad (8)$$

$$\dot{b}_1(t) = \frac{1}{2\omega_1}\left(-\frac{\omega_1^2 b_1(t)}{Q_1} + \frac{3}{4}\beta_1\omega_1^2 a_1(t)(a_1^2(t)+b_1^2(t)) + \frac{\Gamma b_2(t)}{2}\sin(\delta_p t) - \frac{\Gamma a_2(t)}{2}\cos(\delta_p t)\right) \quad (9)$$

where all the off-resonance coefficients have been neglected. Equations (6)–(9) are simultaneously numerically solved using the Runge–Kutta method, and the response of the phonon cavity and the first mode at steady-state can be extracted from $X_2 = \sqrt{a_2^2+b_2^2}$ and $X_1 = \sqrt{a_1^2+b_1^2}$ respectively. The numerical simulations using this formalism can reproduce all the experimental results and are shown in the Supplementary Information.

Noise displacement calibration. The displacement of the first mode is calibrated by normalizing the output signal amplitude at the onset of nonlinearity to the critical displacement and is shown in the Supplementary Information[15]. This yields the responsivity, that is, the change in the output signal per unit displacement $\Re = 0.04$ Am^{-1}. In the proximity of the first mode, a current spectral density limited by the room-temperature amplifier $S_i^{1/2} = 0.9$ pA Hz$^{-1/2}$ is measured, which yields a displacement spectral density $S_{X_1}^{1/2} = S_i^{1/2}/\Re = 22.5$ pm Hz$^{-1/2}$ (ref. 31).

Consequently, white noise corresponding to 1 mV injected into the spectral region around the first mode results in $S_{i_N}^{1/2} = 14$ pA Hz$^{-1/2}$. This yields a noise displacement $X_1' = S_{i_N}^{1/2}\sqrt{\gamma_1}/\sqrt{2\pi}\Re = 0.37$ nm.

Received 7 November 2011; accepted 23 February 2012; published online 1 April 2012; corrected online 26 April 2012

References

1. Kippenberg, T. J. & Vahala, K. J. Cavity optomechanics: Back-action at the mesoscale. *Science* **321,** 1172–1176 (2008).
2. Metzger, C. H. & Karrai, K. Cavity cooling of a microlever. *Nature* **432,** 1002–1005 (2004).
3. Arcizet, O., Cohadon, P. F., Briant, T., Pinard, M. & Heidmann, A. Radiation-pressure cooling and optomechanical instability of a micromirror. *Nature* **444,** 71–74 (2006).
4. Gröblacher, S. *et al.* Demonstration of an ultracold micro-optomechanical oscillator in a cryogenic cavity. *Nature Phys.* **5,** 485–488 (2009).
5. Riviére, R. *et al.* Optomechanical sideband cooling of a micromechanical oscillator close to the quantum ground state. *Phys. Rev. A* **83,** 063835 (2011).
6. Thompson, J. D. *et al.* Strong dispersive coupling of a high-finesse cavity to a micromechanical membrane. *Nature* **452,** 72–75 (2008).
7. Teufel, J. D., Harlow, J. W., Regal, C. A. & Lehnert, K. W. Dynamical backaction of microwave fields on a nanomechanical oscillator. *Phys. Rev. Lett.* **101,** 197203 (2008).
8. Rocheleau, T. *et al.* Preparation and detection of a mechanical resonator near the ground state of motion. *Nature* **101,** 72–75 (2009).
9. Park, Y. S. & Wang, H. Resolved-sideband and cryogenic cooling of an optomechanical resonator. *Nature Phys.* **5,** 489–493 (2009).
10. Teufel, J. D. *et al.* Sideband cooling of micromechanical motion to the quantum ground state. *Nature* **475,** 359–363 (2011).
11. Chan, J. *et al.* Laser cooling of a nanomechanical oscillator into its quantum ground state. *Nature* **478,** 89–92 (2011).
12. Faust, T., Krenn, P., Manus, S., Kotthaus, J. P. & Weig, E. M. Microwave cavity-enhanced transduction for plug and play nanomechanics at room temperature. *Nature Commun.* **3,** 728 (2012).
13. Zakka-Bajjani, E. *et al.* Quantum superposition of a single microwave photon in two different colour states. *Nature Phys.* **7,** 599–603 (2011).
14. Venstra, W., Westra, H. & van der Zant, H. Q-factor control of a microcantilever by mechanical sideband excitation. *Appl. Phys. Lett.* **99,** 151904 (2011).
15. Mahboob, I. & Yamaguchi, H. Bit storage and bit flip operations in an electromechanical oscillator. *Nature Nanotech.* **3,** 275–279 (2008).
16. Mahboob, I., Flurin, E., Nishiguchi, K., Fujiwara, A. & Yamaguchi, H. Interconnect-free parallel logic circuits in a single mechanical resonator. *Nature Commun.* **2,** 198 (2011).
17. Weis, S. *et al.* Optomechanically induced transparency. *Science* **330,** 1520–1523 (2010).
18. Safavi-Naeini, A. H. *et al.* Electromagnetically induced transparency and slow light with optomechanics. *Nature* **472,** 69–73 (2011).
19. Gröblacher, S., Hammerer, K., Vanner, M. R. & Aspelmeyer, M. Observation of strong coupling between a micromechanical resonator and an optical cavity field. *Nature* **460,** 724–727 (2009).
20. Teufel, J. D. *et al.* Circuit cavity electromechanics in the strong-coupling regime. *Nature* **471,** 204–208 (2011).

21. De Liberato, S., Lambert, N. & Nori, F. Quantum noise in photothermal cooling. *Phys. Rev. A* **83,** 033809 (2011).
22. Marquardt, F., Chen, J. P., Clerk, A. A. & Girvin, S. M. Quantum theory of cavity-assisted sideband cooling of mechanical motion. *Phys. Rev. Lett.* **99,** 093902 (2007).
23. Wilson-Rae, I., Nooshi, N., Zwerger, W. & Kippenberg, T. J. Theory of ground state cooling of a mechanical oscillator using dynamical backaction. *Phys. Rev. Lett.* **99,** 093901 (2007).
24. Lambert, N., Johansson, R. & Nori, F. A macro-realism inequality for opto-electro-mechanical systems. *Phys. Rev. B* **84,** 245421 (2011).
25. O'Connell, A. D. *et al.* Quantum ground state and single-phonon control of a mechanical resonator. *Nature* **464,** 697–703 (2010).
26. Rodrigues, D. A. Fano-like antiresonances in nanomechanical and optomechanical systems. *Phys. Rev. Lett.* **102,** 067202 (2009).
27. Agarwal, G. S. & Huang, S. Electromagnetically induced transparency in mechanical effects of light. *Phys. Rev. A* **81,** 041803 (2010).
28. Schliesser, A. & Kippenberg, T. J. Cavity optomechanics with whispering-gallery mode optical micro-resonators. *Adv. At. Mol. Opt. Phys.* **58,** 207–323 (2010).
29. Mahboob, I., Wilmart, Q., Nishiguchi, K., Fujiwara, A. & Yamaguchi, H. Wide-band idler generation in a GaAs electromechanical resonator. *Phys. Rev. B* **84,** 113411 (2011).
30. Westra, H. J. R., Poot, M., van der Zant, H. S. J. & Venstra, W. J. Nonlinear modal interactions in clamped-clamped mechanical resonators. *Phys. Rev. Lett.* **105,** 117205 (2010).
31. Mahboob, I., Flurin, E., Nishiguchi, K., Fujiwara, A. & Yamaguchi, H. Enhanced force sensitivity and noise squeezing in an electromechanical resonator coupled to a nanotransistor. *Appl. Phys. Lett* **97,** 253105 (2010).
32. Dobrindt, J. M., Wilson-Rae, I. & Kippenberg, T. J. Parametric normal-mode splitting in cavity optomechanics. *Phys. Rev. Lett.* **101,** 263602 (2008).
33. Massel, F. *et al.* Microwave amplification with nanomechanical resonators. *Nature* **480,** 351–354 (2011).
34. Santamore, D. H., Doherty, A. C. & Cross, M. C. Quantum nondemolition measurement of Fock states of mesoscopic mechanical oscillators. *Phys. Rev. B* **70,** 144301 (2004).

Acknowledgements

The authors are grateful to S. Miyashita for growing the heterostructure, A. Fujiwara for support and N. Lambert, P. D. Nation and F. Nori for discussions and comments. This work was partly supported by Japan Society for the Promotion of Science (JSPS) KAKENHI (20246064) and (23241046).

Author contributions

I.M. conceived the experiment, designed and fabricated the electromechanical resonator, performed the measurements, analysed the data and wrote the paper. K.N. designed and fabricated the Si-nanoFET amplifiers. H.Y. planned the project. All authors discussed the results.

Additional information

The authors declare no competing financial interests. Supplementary information accompanies this paper on www.nature.com/naturephysics. Reprints and permissions information is available online at www.nature.com/reprints. Correspondence and requests for materials should be addressed to I.M. or H.Y.

CORRIGENDUM

Phonon-cavity electromechanics

I. Mahboob, K. Nishiguchi, H. Okamoto and H. Yamaguchi

Nature Physics **8,** 387–392 (2012); published online 1 April 2012; corrected after print 26 April 2012.

In the version of this Letter originally published, the name of the first author of ref. 21 should have read 'De Liberato, S.'. This error has been corrected in the HTML and PDF versions of the Letter.